Chapter 5

Highly efficient broadband metamaterial absorber using GaAs split-disk resonators

In this chapter, we have explored an efficient ultrathin broadband metamaterial (MTM) solar absorber design to enhance the efficiency of solar energy harvesting devices. The proposed absorber shows a usual absorption of 96.57% in the 375 nm to 1200 nm region. The simulated MTM absorber consists of only two layers of gallium arsenide and tungsten. The dielectric layer of GaAs is used as a metasurface (resonator) over a ground layer of tungsten. The absorber exhibits polarization-independent behaviors for a wide range of incident angles for TE and TM modes. The proposed absorber can be utilized as an ultrathin compact solar energy absorber device with efficient solar radiation absorptivity.

5.1 Introduction

Realizing a wide-band perfect metamaterial absorber is the primary goal of this thesis. In previous chapters, we discussed precision metamaterial absorber designs consisting of three layers that demonstrated and characterized wide-band response capable of tuned broadband. In this chapter, a new wide-band tunable polarization, and incident angle insensitive perfect metamaterial with only a two-layer structure is proposed as a goal to achieve the absorber. One benefit of the suggested design is that it offers a high degree of symmetric flexibility, allowing it to deliver resonant absorption close to a unit with good absorption. The proposed absorber can be improved efficiency which can be used for applications related to solar energy.

The advancement of harnessing renewable energy to electric power generation technologies is immensely crucial to preserving the global environment, and energy demands of today's society, and assuring sustained economic growth. Solar energy is one of the most effective and promising renewable energy sources for directly converting sunlight into electrical energy. In the 1920s, cuprous oxide (Cu_2O) semiconductors attracted much attention for solar cell applications due to their high capacity, low cost, and economical fabrication [201,202]. Because the cuprous oxide is a semiconductor and shows the direct bandgap (2.1eV) that is suitable for photovoltaic conversion. However, this semiconductor achieves poor efficiency due to its low absorption of solar radiation [203]. Recently, metamaterial absorber technology has attempted to increase the efficiency of photovoltaics by absorbing solar radiation effectively. Because of the low cost, lightweight, and flexibility, researchers have focused their efforts on solar cells with a thickness of a few micrometers or less [204,205]. Weak

light absorption is one of the primary issues with thin-film solar cells. As a result, a light-trapping structure is frequently necessary to improve Light absorption.

The first metamaterial absorbance was presented in the year 2008 by Landy et al.[68] and this absorber reveals the negative property of permeability and permeability of a metamaterial. As a result, they achieved a 88% absorption rate at a frequency of 11.5 GHz. Later, many researchers reported the absorption in different frequency ranges for the visible and microwave regions. The properties of metamaterials depend on their material or physical structures and can be tuned with their relative parameters. Metamaterial (MTM) absorber exhibits exotic properties such as negative effective permeability and permeability that cannot be found in conventional and natural absorbers [6]. Metamaterials have been utilized to design various potential devices such as antenna [112], super-lens [206], invisible clock [207], absorbers [191,208], imaging [209], and sensor [210], respectively. Moreover, metamaterials have also been used to develop different types of highly efficient electromagnetic wave absorbers [160,211]. The maximum absorption has been reported by the periodic structure of the metamaterial absorber [212]. An absorber can be said to be an ideal absorber only if it can absorb all the incident electromagnetic waves, and their reflection, transmission, and scattering become negligible in this phenomenon[91]. In recent years, many researchers have presented various metamaterial absorbers to achieve perfect absorption, such as single to multiband [129,139,213] and broad absorption bands [116,122].

Metamaterial absorber promises to be a highly efficient and wideband absorber design for different potential applications. A thin sheet of a photovoltaic cell made of metamaterials can be easily used and folded according to their utility. Solar thermo-photovoltaics with

metamaterial will be highly useful for future applications as their efficiency can exceed a current maximum value. Therefore, many researchers have turned their attention to demonstrating the different types of metamaterial devices. Various metals have been used in metamaterial absorbers to achieve perfect absorption [214]. Conventional plasmon metals such as gold, silver, aluminum, and copper have weak thermal stability and loss of single resonance frequency, while the new plasmon metal of tungsten (W) exhibits a higher thermal melting point and wide resonance frequency. The high melting point of tungsten metal can help the absorber withstand the higher temperature when absorbing significant photons of higher energy. Tungsten metal is applicable for producing perfect broadband absorbers at a low cost. In addition, short-circuit current density (J_{sc}) is an essential parameter in solar cells. Short-circuit current density is utilized to characterize the maximum current administered by a solar cell and depends on the optical properties of the solar cell [215,216]. The charge separation driving force is represented by the open-circuit voltage (V_{oc}), which is one of the solar cell characteristics [217]. The potential difference of electrons is represented by a voltage. V_{oc} is expected to be significant due to the large pushing force of charge separation.

In this study, we report a novel metamaterial absorber structure for solar energy harvesting applications that exhibits ultra-broadband, wide-angle and polarization-independent absorption. Tungsten metal-based absorbers provide near-unity absorption (>99%) and cover a large portion of the electromagnetic spectrum from the visible to the NIR region. The absorber provides perfect absorption due to matching the impedance with free space, which is the primary factor for achieving near-unity absorption. The performance of parametric studies of a unit cell is also discussed. In addition, we have analyzed absorption spectra with different

incident angles and observed polarization-independent absorption performance. For both modes at different angles (0^0 to 50^0) at 10^0 intervals, we have obtained an average absorption of 95.41% and 96.88%. We have obtained high short-circuit current densities with various incident angles for TE and TM under AM1.5G solar illumination. Further, we have also revealed the open-circuit voltage (V_{oc} =0.72 V), fill factor (84.85%), and conversion efficiency (η = 27.33%), respectively. Therefore, the proposed absorber can be employed for various highly efficient solar harvesting devices, and thin-film photovoltaic cells.

5.2 Geometry, Parameters, Simulation Setup, and Methods

5.2.1 Design and geometry, parameters of unit cell structure

We have presented a novel structure of metamaterial absorber, which is made up of only two-layer. Tungsten (W) metal has been used as the ground layer, and the dielectric of gallium arsenide (GaAs) has been adopted as the metasurface. Tungsten metal shows a high melting point and better response under high temperatures. The parameters of the structure are periodicity of 400 nm, the bottom layer thickness (t_1) of 200 nm and the top layer (t_2) of 100 nm, the radius of the circle (r) of 170 nm, and the gap (g) of 28 nm. Fig. 5.1 depicts the schematic view of a unit cell of the investigated structure. Among the proposed absorbers, gallium arsenide (GaAs) is an important semiconductor material used to produce highly efficient solar cells. GaAs material has been greatly used because of its prominent properties such as high saturated electron velocity, high electron mobility, and wide energy band gap, which made it most efficient for high-temperature devices. Furthermore, GaAs show a direct band gap that makes them good solar energy absorbers [218]. The GaAs's specifications are ε = 12.94, tanδ = 0.006, Rho = 5320 [kg/m^3], and thermal conductivity = 54 [W/K/m]. The spacer

has low noise, saturated electron velocity, high electron mobility, and a high-temperature range for the wide bandgap. These important properties are the region for selecting the GaAs as a resonator in the proposed design. Therefore, it is an excellent material for the absorption of solar radiation [146]. The fabrication process of the proposed absorber can be easily done by using popular nanofabrication techniques such as nano-imprinting lithography and e-beam lithography [219].

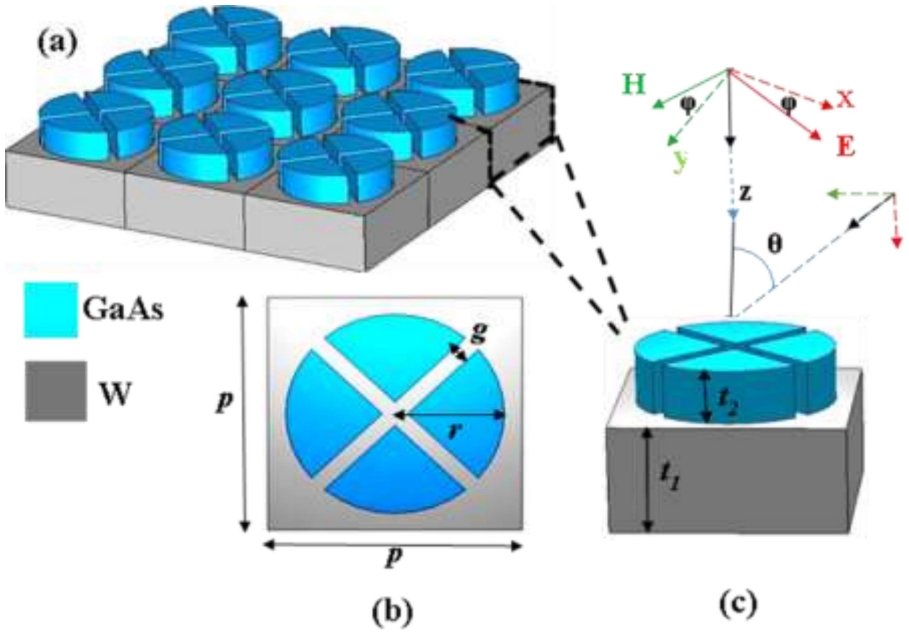

Fig. 5.1 (a) Schematic diagram of the proposed metamaterial absorber, **(b)** front view, **(c)** magnified view of one of its unit cells.

5.2.2 Simulation setup

To obtain absorption spectra at a normal incidence angle in the wavelength range of 375 nm - 1200 nm, periodic boundary conditions have been applied in the direction of the x and y axis, while the Floquet ports are assigned to the z-direction, respectively. The incoming wave's polarisation was chosen so that the electric ($\vec{E}$) and magnetic ($\vec{H}$) fields travel in parallel with

the absorber's geometric plane, whereas a linearly polarised incidence would be normal to the metamaterial structure. CST Microwave Studio, a commercial 3D electromagnetic simulator, has been used to perform numerical calculations based on the FIT (Finite Integration Technique) method [220]. A frequency-domain solver has been used to analyze all the data.

5.2.3 Absorption characteristics

Eq. 5.1 can be used to compute the absorbance of the suggested absorber, where A(ω), R(ω), and T(ω) indicate absorption, reflectance, and transmittance, respectively. T(ω) is not considered in the equation because the bottom layer of the absorber eliminates the transmitted waves, so it cannot pass power. Therefore, Eq. 5.1 can be changed into Eq. 5.2 with the scattering parameter (S_{11} = R(ω)) [221],

$$A(\omega) = 1 - R(\omega) - T(\omega) \tag{5.1}$$

$$A(\omega) = 1 - \left| S_{11}(\omega) \right|^2 \tag{5.2}$$

The absorption behavior can be better understood by the effective impedance matching method, for which the impedance matching between the absorber and the surrounding medium is very important. The effective impedance (z_{eff}) is a complex value that can be written as real and imaginary impedance and the relationship between the scattering parameters (S_{11} and S_{21}) and the impedance can be expressed as Eq. 5.4. The parametric retrieval method helps to calculate the impedance of the absorber using s-parameters [222]. Furthermore, the absorbance (A) of the absorber can be depicted as the real part $Re(z)$ and the imaginary part $Im(z)$ of z_{eff}, as shown in Eq. 5.5 [223]. Data purification has been done by using CST-MATLAB.

$$z_{eff} = \mathrm{Re(z)} + i.\mathrm{Im(z)} \tag{5.3}$$

$$z_{eff} = \pm\sqrt{\frac{(1+\mathrm{S_{11}})^2 - \mathrm{S_{21}^2}}{(1-\mathrm{S_{11}})^2 - \mathrm{S_{21}^2}}} \tag{5.4}$$

$$\mathrm{A(\omega)} = \frac{4\mathrm{Re(z)}}{[1+\mathrm{Re(z)}]^2 + [\mathrm{Im(z)}]^2} \tag{5.5}$$

According to Eq. 5.5, if the metamaterial acquires a near-unity absorber (A) at absorber wavelengths, then the corresponding *Re(z)* of the effective impedance should be close to 1, and the *Im(z)* of the effective impedance should be close to 0, respectively. Fig. 5.2(b) depicts the real and imaginary sections of the suggested absorber's impedance which are in the range of wavelengths (375 nm -1200 nm) around 1 and 0, respectively which indicates that the optimum impedance of the best absorber is well-matched to that of the surrounding medium.

5.3 Result and Discussion

5.3.1 Impedance and the absorbance of the proposed absorber

We have proposed two layer-based metamaterial absorbers consisting of a tungsten (W) layer as the ground layer and a gallium arsenide (GaAs) layer as the top layer (resonator). Fig. 5.2(a) shows absorption results in which the tungsten layer achieves an average absorption of 50.04% and the gallium arsenide layer 10.93%. The contribution of both the layers (front and back) gives high absorption indicating a good absorber design. The red curve depicts the absorption of the provided absorber (two layers), while the blue and green curve depicts the absorption of the substrate (tungsten metal) and split disk of the GaAs layer in the wavelength range of 375 to 1200 nm. Fig. 5.2(b) shows the impedance curve of the split disk layer (GaAs) and the proposed structure. The impedance of the GaAs layer is very high, which is not close to the

unit impedance of the free space, due to which the GaAs layer cannot achieve much absorption. The high intrinsic loss of the back-layer (tungsten) makes the resonance stronger and contributes towards the absorption of the structure composed of GaAs and W layers. The combined effect of both layers is directly responsible for this ultra-high absorption. The key principle of absorption is impedance matching and surface plasmonic resonance. Therefore, high absorption is the result of impedance matching with the free space, which can be endorsed by the resonance of the front layer and the intrinsic loss of the back layer. The red curve shows the impedance of the unit cell in Fig. 5.2(b), which yields absorption due to its proximity to the air impedance. In this broadband region, the proposed structure achieves 99.84% absorbance at 482.85 nm and more than 99.50% absorbance at 566.87 nm, 756.47 nm, and 857.65 nm. The average absorbance in the 375 nm to 1200 nm wavelength range is 96.57%. We observe a higher absorption bandwidth which is rarely found in the 410 nm to 1200 nm wavelength region. We observe that the proposed two-layer based absorber is cost-efficient and compact in size with a high absorption rate as compared to the previously reported four-layer[224,225], and three layers[129,131] based MTM absorber.

The proposed broadband absorber is composed of a gallium arsenide layer (GaAs) on a tungsten substrate, and the surrounding region is considered to be air. Fig. 5.2(c) shows two absorption spectra at normal incidence. The blue-colored curve represents the absorption of a perfect disk, and the red-colored curve expresses the absorption of a split disk structure of the unit cell. The perfect circular disk and split disk structures represent the 90.85% and 96.57% average absorption. The impedance of the structure with the GaAs split resonator is relatively higher than that of the perfect disk, due to which the structure with the GaAs split resonator

achieves an almost perfect absorption rate in the considered wavelength range [226]. The perfect disk resonator of GaAs shows two absorption peaks formed due to the field coupling between the structures. When the impedance of the metamaterial structure is close to the impedance of the free space, the structure exhibits good absorption. As the impedance of the metamaterial structure moves away from the impedance of the free space, the absorption gradually decreases. Fig. 5.2(d) shows the impedance of the perfect disk and the split disk design structure of the unit cell. The parameters have a significant impact on the geometric shape to meet the impedance, and the geometric structure has an impact on the absorption. Thus, the split disk resonator-based metamaterial shows better absorption than the perfect disk resonator.

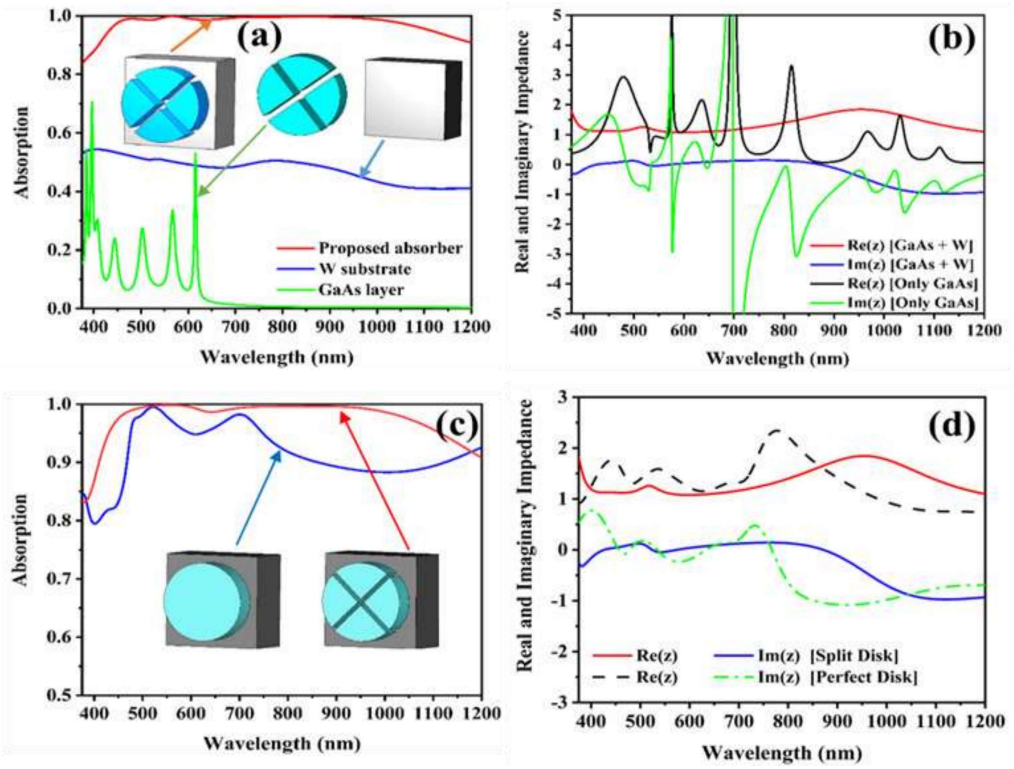

Fig. 5.2 (a) Absorption spectrum of a substrate, GaAs split disk, and proposed unit cell, **(b)** normalized effective impedance of only GaAs split disk and proposed unit cell, **(c)** absorption spectra with perfect disk and split disk unit cells, **(d)** normalized effective impedance of perfect disk and split disk unit cells**.**

5.3.2 Effect of Co-polarization and Cross-polarization on absorption

For metamaterial absorbers, one question still arises whether the unit cell should not serve as a polarization converter and give a polarization conversion ratio (PCR) value instead of an absorbance. Due to the twofold symmetrical structure, we have illustrated the co-polarization reflection coefficient (R_{xx} and R_{yy}), and the cross-polarization coefficient (R_{xy} and R_{yx}) in Fig. 5.3(a). These coefficients can be measured from Eqs. 5.6 and 5.7,

$$\left|S_{11}(\omega)\right|^2 = \left|R_{yx}\right|^2 + \left|R_{yy}\right|^2 \tag{5.6}$$

$$\left|S_{11}(\omega)\right|^2 = \left|R_{xy}\right|^2 + \left|R_{xx}\right|^2 \tag{5.7}$$

As a magnitude (dB) scale, the cross-polarization reflection coefficients are almost zero, which can be easily seen in Fig. 5.3(a), and ensures that the unit cell has not converted waveforms. PCR can be calculated from Eqs. 5.8 and 5.9 which are used as linear values of the coefficient components. From Fig. 5.3(b), it can be understood that the polarization does not change by the design of the wave absorber, and for both modes (TE and TM), the PCR value is almost zero [227,228]. Excellent symmetry is the primary reason for this type of result.

$$PCR_{TE} = R_{yx}^2/(R_{yx}^2 + R_{yy}^2) \tag{5.8}$$

$$PCR_{TM} = R_{xy}^2/(R_{xy}^2 + R_{xx}^2) \tag{5.9}$$

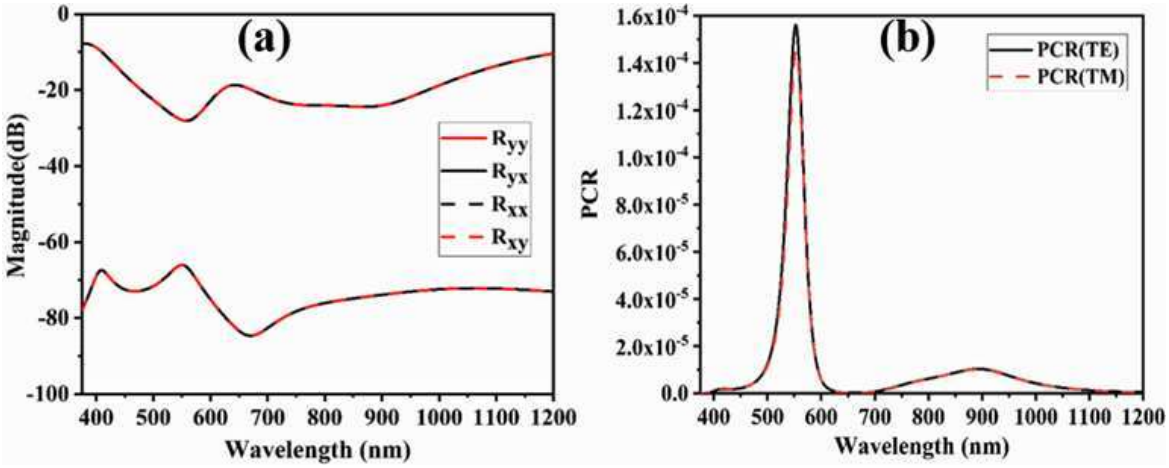

Fig. 5.3 (a) Magnitude (dB) component of co-polarization and cross-polarization, **(b)** PCR (polarization conversation ratio) for TE and TM modes.

5.3.3 Parametric study of a unit cell

In this section, we have observed different absorption spectrums sweeping the geometrical parameters of the structure. Here, the optimized period (p), GaAs thickness (t_2), radius (r), and gap (g) are 400 nm, 100 nm, 170 nm, and 28 nm, respectively. The variable absorption spectra with different periods of the optimized structure are exhibited in Fig. 5.4(a). As the periodicity decreases, absorption increases in the near-infrared region while decreases in the visible region. On the other hand, as the periodicity increases, absorption decreases in the near-infrared region while it increases in the visible region [229]. Thus, the ideal absorption can be achieved by repeatedly changing the period (p). The effect of the resonator thickness (t_2) on the absorption spectra is shown in Fig. 5.4(b). The maximum absorption first increases near the optical region and then decreases. In contrast, minimum to maximum absorption is achieved in the optical field, which can be explained using comparable LC circuit theory [230]. In this case, the relevant inductance (L) increases with a thickness (t_2) and decreases the absorption frequency. When the gap (g) increases from 20 nm to 36 nm by an interval of 4 nm,

the actual absorption frequency range gradually changes as demonstrated in Fig. 5.4(c). In this case, the observed resonance frequency of absorption increases with decreasing capacitance (C) as the gap increases. When *g* is less than 28 nm, then the bandwidth of absorption gradually reduces. In addition, strong absorption shifting is observed when increasing the radius (*r*) from 150 nm to 190 nm with an interval of 10 nm as shown in Fig. 5.4(d). As the equivalent inductance and capacitance increase with radius (*r*), the observed absorption frequency decreases. These results represent the geometrical parametric effects for the proposed absorber. We obaserve overall good absorption results with the variation of geometrical parameters of the absorber. Therefore, we can conclude that the optimized full broadband absorber (shown in Fig. 5.2 (a)) exhibits a larger fabrication tolerance than that discussed above.

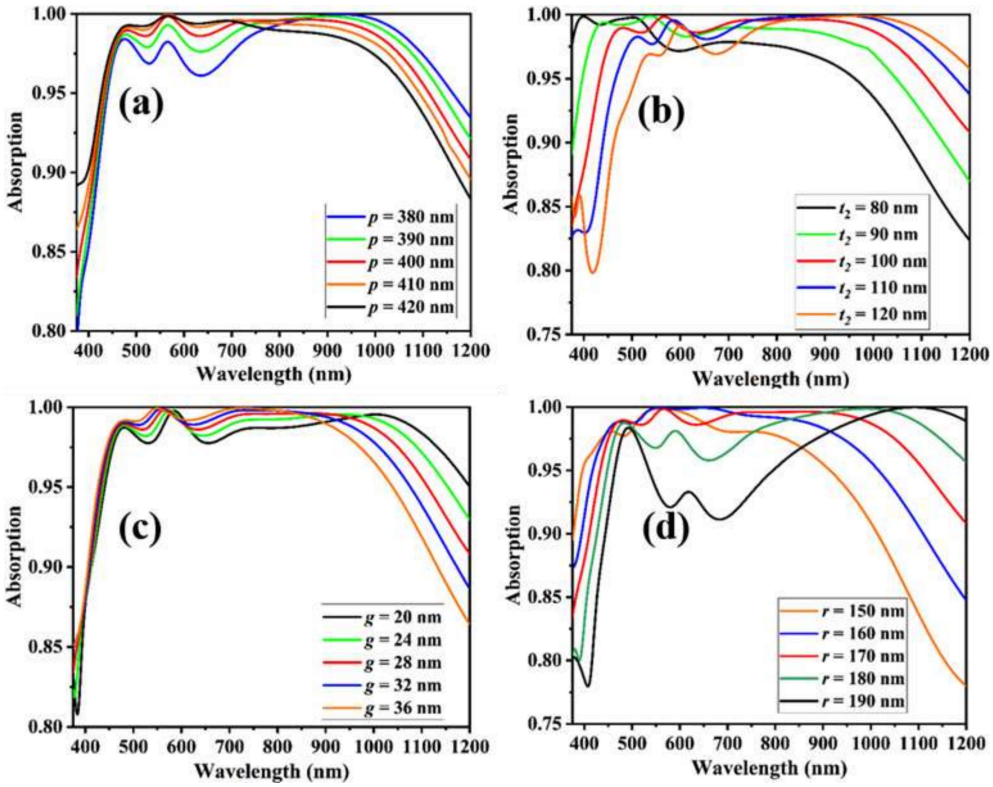

Fig. 5.4 Absorption spectra for different geometry **(a)** periodicity of a unit cell, **(b)** thickness effect of GaAs, **(c)** gap width, **(d)** radius effect.

5.3.4 Absorption performance with polarization angles

The influence of polarization direction on the absorber with normal incidence has been explored in this section. The polarization direction along the x-direction (transverse electric polarization) and y-direction (transverse magnetic polarization) means that the polarization angle is equal to 0^{o} and 90^{o}. Fig. 5.5(a) and 5.5(b) exhibit the absorption spectrum for TE and TM modes. We observe the constant absorption values at the different polarization directions, which is because of the symmetry of the geometry [231]. The polarization independence of the absorber represents stable absorption. These characteristics make the absorber useful in optoelectronics, particularly in the field of solar energy.

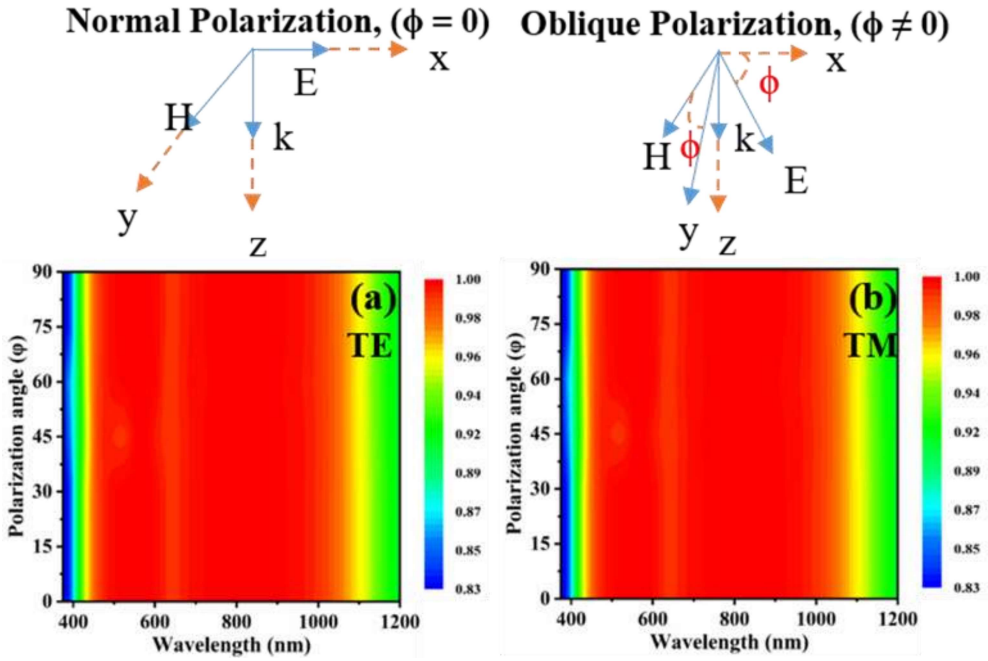

Fig. 5.5 Visual representation of polarization angle (φ) for **(a)** TE mode, **(b)** TM mode.

5.3.5 Absorption performance with incident angles

Furthermore, we have also analyzed the absorption at the normal and oblique incident angles which is another characteristic of the metamaterial absorber. A good absorber performance should not be out of gear with different incident angles of sources. This property helps a lot in which the device is intended to be used. In this case, we have observed the absorption performance at different angles for both modes. At oblique events, the angle of incidence and refraction have a profound effect on the coefficient of reflection, which can be written as [232],

$$\Gamma_{\perp} = \frac{Z_m \text{Cos}\,\theta_i - Z_o \text{Cos}\,\theta_t}{Z_m \text{Cos}\,\theta_i + Z_o \text{Cos}\,\theta_t} \tag{5.10}$$

$$\Gamma_{\parallel} = \frac{Z_m \text{Cos}\theta_t - Z_o \text{Cos}\theta_i}{Z_m \text{Cos}\theta_t + Z_o \text{Cos}\theta_i} \tag{5.11}$$

Where Z_o is the impedance of free space and Z_m is the impedance of the absorber. Similarly, θ_t is the transmitting angle and θ_i is the incidence angle. Hence, according to Snell's law,

$$\frac{Z_o}{Z_m} = \frac{\text{Sin } \theta_t}{\text{Sin } \theta_i} \tag{5.12}$$

By solving Eqs. 5.10 and 5.11 with the help of Eq. 5.12, we can get the maximum absorption for both polarization modes,

$$A_{TE} = \varepsilon\mu - \varepsilon^2 sin^2\theta_i - \mu^2 cos^2\theta_i = 0 \tag{5.13}$$

$$A_{TM} = \mu - \varepsilon\, sin^2\theta_i - \mu\varepsilon\, cos^2\theta_i = 0 \tag{5.14}$$

We obtained distinct absorption spectrums for both modes (TE and TM) at different angles to compute the absorbance performance, as shown in Fig. 5.6(a) and 5.6(b). The angle of incidence increased by an interval of 10° from 0° to 50°. When the incidence is below 50°, the average absorbance in TE mode stays over 90%, as illustrated in Fig. 5.6(a). Because resonant modes associated with the electric field component cannot be generated effectively beyond 50°, the absorbance steadily declines with increasing incidence angle. The suggested absorbers achieve more than 90% average absorption over a wide incident angle as illustrated in Fig. 5.6(b) for the TM mode. This is because the excitation of the resonance mode associated with the components of the magnetic field can remain practically unchanged. The broadband absorption performance of TM mode is less reliant on the incidence angle than that of TE mode given the intended structure of the absorber. The average absorption for TE and TM modes is 95.41 percent and 96.88 percent, respectively [233]. As a result, the suggested absorber's simple

design makes it a strong candidate for the construction of efficient optical devices working in the visible regime at wide incident angles.

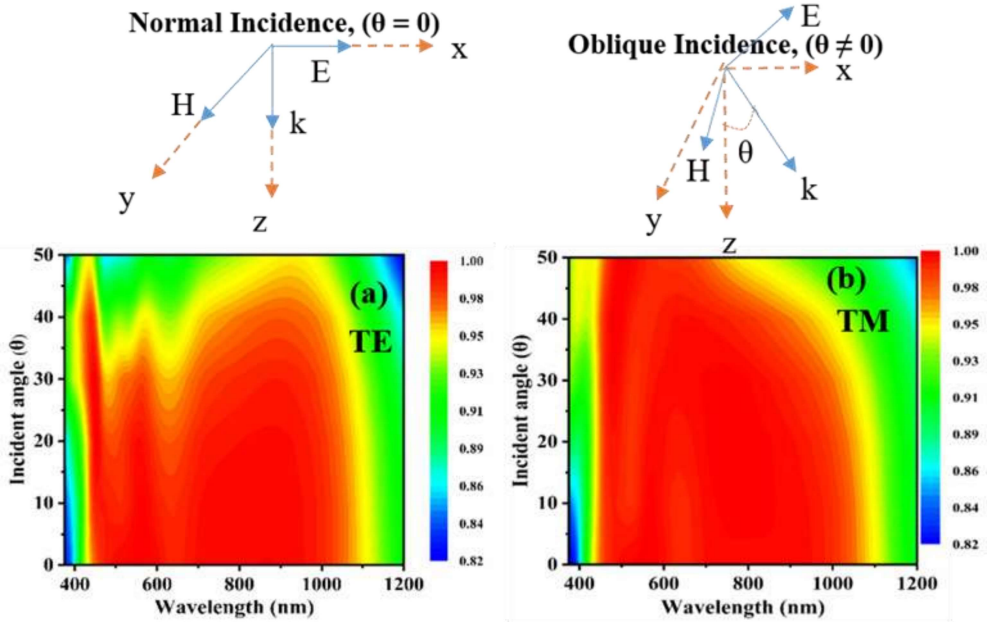

Fig. 5.6 Absorption spectra at the various incident angle (θ) from 0º to 50º for **(a)** TE mode, **(b)** TM mode.

5.3.6 Absorption performance with different metals and dielectric layers

Further, we have also analyzed the absorption performance of the proposed structure with different dielectric materials and metals. Fig. 5.7(a) reveals the absorption spectra for various bottom metals. When we replaced the metal of tungsten (W) with ideal metals such as gold (Au), and silver (Ag), and refractory metals such as nickel (Ni), and chromium (Cr), it was observed that absorption in the broadband region of the spectra changes. The absorption spectra exhibit two narrow resonances at 400 nm and 500 nm for noble metals. However, when using lossy refractory metals, the absorber provides strong absorption because it appreciates and satisfies the thickness and matches the impedance conditions. The slight metal loss is

responsible for the narrow bandwidth [234]. Fig. 5.7(b) exhibits the absorption performance of the proposed absorber for different dielectric materials (SiO_2, SiN, A-Si, and GaAs). The bandwidth and intensity of absorption become more extensive with increasing the dielectric constants of the constituted dielectric materials in the absorbers. Therefore, we have obtained a higher bandwidth and absorption for a low dielectric constant due to the limitation of fields [235].

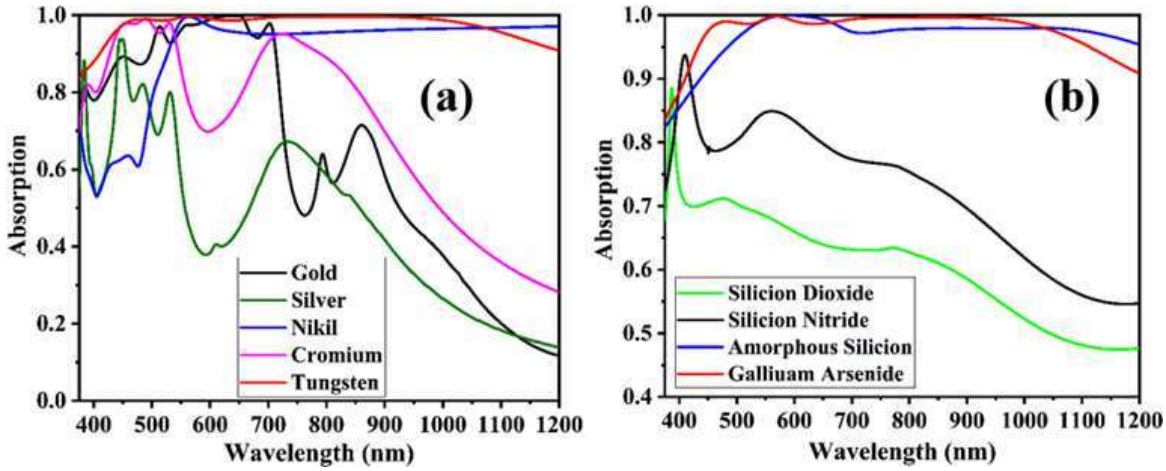

Fig. 5.7 Absorption spectra with various **(a)** metals, **(b)** semiconductor materials.

5.3.7 Short circuit current density of the proposed absorber

For the TE and TM modes, the short-circuit current density (J_{sc}) has been determined at various incident angles. The J_{sc} is calculated by integrating the absorbance with solar illumination of global air mass 1.5 (AM1.5G), assuming that all produced electron-hole pairs contribute to the current [148]. J_{sc} can be calculated with the help of Eq. 5.15,

$$J_{sc} = \int_{375\ \mathrm{nm}}^{1200\ \mathrm{nm}} \frac{q\lambda}{hc} A(\lambda) I_{AM1.5} I(\lambda)\, d\lambda \tag{5.15}$$

Where q is an electron's charge, λ is the wavelength of light, h is the Plank's constant, c is the speed of light, $I_{AM1.5}(\lambda)$ is solar radiance under the AM1.5, and A(λ) is the absorbance. Fig. 5.8(a) shows the influences of J_{sc} under different incident angles at the steps of 10° angle. The higher value of J_{sc} is obtained at the normal incidence angle for both modes. All values of short-circuit current density are tabulated in Table 5.1. When the angle of incidence of the absorber is tuned from 0^{o} to 80^{o} with a step of 10^{o}, the change in J_{sc} is not regular. This is because J_{sc} is mostly determined by the number of resonant modes created in the wavelength region. We have obtained the best value of J_{sc} (44.75 mA/cm^2) at the normal incident angles for both modes which is much larger than previously reported work [199]. Usually, solar energy efficiency has been studied to evaluate the solar absorption response of absorbers. The perfect absorber has a near-unity absorption band over a large wavelength range. Here, we explore solar absorption by applying the illumination of the solar radiation AM1.5 source [146]. The absorption under the solar radiation AM1.5 and missed solar energy of this absorber is depicted in Fig. 5.8(b). Even when light collection efficiency is extremely high, some energy is lost. Due to its resonant response over a wide frequency range and multiple resonance coupling, this absorber captures near-unity solar energy. As a result, optoelectronic devices can benefit from the proposed absorber.

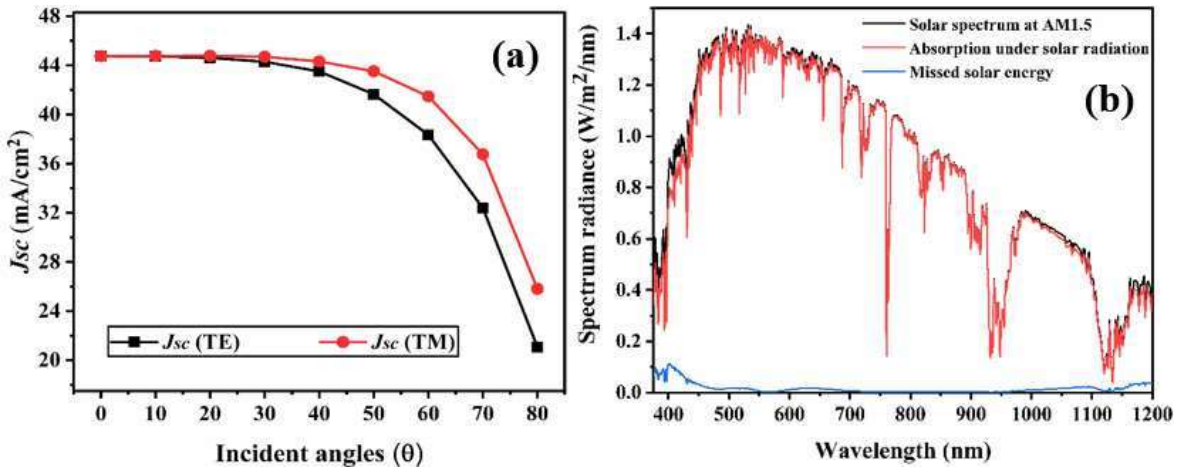

Fig. 5.8 Effect of **(a)** short-circuit current density for TE and TM modes with various incident angles (0°-80°), **(b)** standard spectrum of solar radiance AM1.5, absorption under solar radiation and missed solar energy for the wavelength region 375nm -1200 nm.

Table 5.1 The short-circuit current density (J_{sc}) with various incident angles.

θ°	0°	10°	20°	30°	40°	50°	60°	70°	80°
***Jsc* (TE)**	44.75	44.74	44.61	44.29	43.50	41.64	38.33	32.38	21.07
***Jsc* (TM)**	44.75	44.76	44.78	44.70	44.31	43.51	41.47	36.75	25.81

5.3.8 Electric field and Magnetic field analysis

We investigate the distribution of electric and magnetic field distributions in unit-cell metamaterial structures to understand better the physical nature underlying the absolute broadband absorption of the developed absorber. The electromagnetic field distributions affect the absorption properties of the absorber for the TE and TM modes. The field distributions of the absorber in the x-y plane at two different wavelengths (λ = 482.85 nm and 857.65 nm) are shown in Fig. 5.9. At these wavelengths, we observe the maximum absorption, so we have considered these wavelengths. The figure shows the distribution of the electric field at the

wavelengths of 482.85 nm and 857.65 nm. We observe that the strong electric field is concentrated in the inner gap of the disk and outer parts of the split disk, which indicates that a significant electrical resonance activates in the GaAs split disk. It observes that the electric field originates outwards from the top of the split disk and is located in the air above the disk, which indicates that the surface lattice resonance is generated when strong electrical resonance is excited. According to the electric field distribution, as shown in Fig. 5.9 (a, c), the strong coupling of the electric field is the primary cause of the absorption peak. The interactions between the electric fields on the inner gap and the outer surfaces of the disk overlap, thereby strengthening the coupling between them. Near the surface of the metal substrate, we also observe a reasonably strong electric field. As a result of this phenomenon, it may be inferred that the propagating plasma resonance mode is also excited close to the tungsten film. Fig.5.9 (b, d) shows the magnetic field distribution at 482.85 nm and 857.65 nm wavelengths. At 482.85 nm wavelength, it shows a strong magnetic field located in both directions x and y of the GaAs split disk, while GaAs split disk exhibits strong magnetic hot spots at 857.65 nm wavelength on both sides of the x and y direction. These characteristics show that the structure has strong magnetic resonance excitation. Meanwhile, the magnetic field increases in the GaAs split disk and the metal surface between the split disks. The complete absorption is the result of the strong magnetic resonance of the split disk and the interaction with the metal surface. The magnetic field distribution within the disk gap and on the metal surface suggests that magnetic field coupling caused the absorption peak. At these resonant wavelengths, the optical field distribution shows that electric and magnetic resonances, as well as the field coupling effects present in GaAs absorbers, lead to broadband light absorption [226,236115].

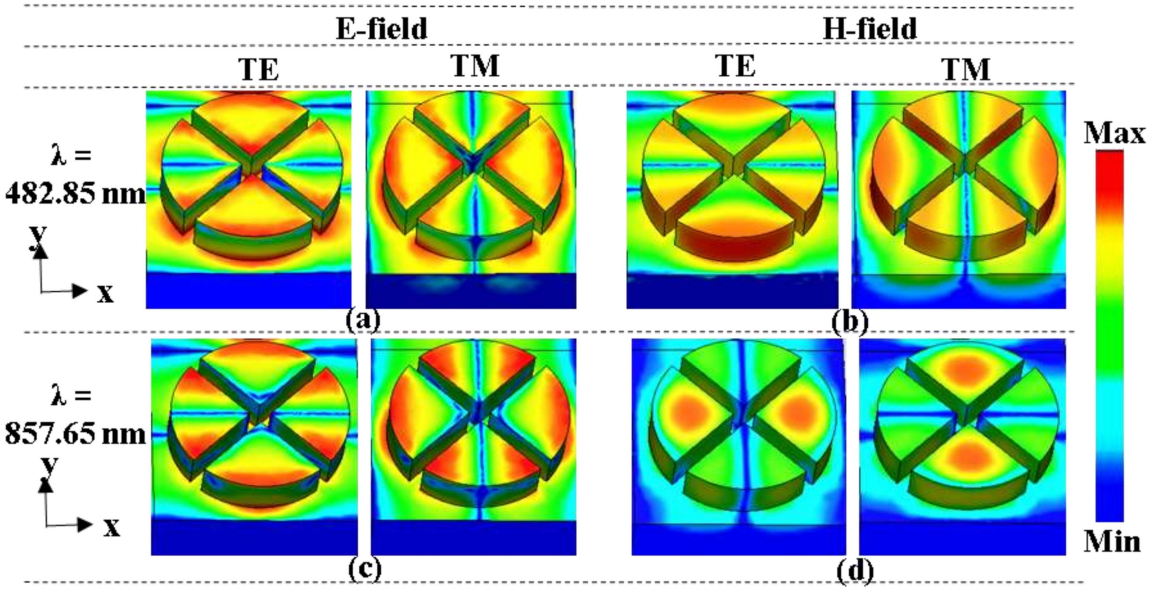

Fig. 5.9 Distribution of the electric field **(a, c)** and the magnetic field, **(b, d)** in the unit cell for the TE and TM modes for wavelengths 482.85 nm and 857.65 nm on the y-x plane.

5.3.9 Comparative study

As mentioned earlier, the metamaterial absorber covering the wide region from 375 nm to 1200 nm is highly desirable. Table 5.2 represents a comparison of the previously reported designs with our proposed design. Where *l*, *b,* and *h* represent the length, breadth, and height of a unit cell, respectively. By looking at the table, one can easily conclude that our proposed work surpasses the absorption results of the previously reported work with wide angles. Our proposed absorber operates from the visible to a near-infrared region with 96.57% average absorption. A good impedance of the absorber is the main reason for its higher absorption. We have used cost-effective tungsten metal for designing the ground layer of our proposed design and obtained better results as compared to the previously reported design which has used costlier metals such as Ag and Au. In the table, we have compared three-layer[193,237] and two-

layer[115,166,226] based MTM absorbers with standard features like dimensions, bandwidth layer, used materials, peak values, absorption level, and different incident angles.

Table 5.2 A comparison of the suggested absorber to previously published work.

Bandwidth (nm)	Dimensions (l×b×h)	No. of layers	Used Materials	Peak values (%)	Absorption (%)	Ref.#
300	380×380×30	Three	Ag, SiO_2	98	Above 90	193
300	250×250×95	Three	Ni, Si	99	Above 90	237
400	240×240×70	Two	Au, Si	99.1	Above 90	166
220	300×300×60	Two	Au, GaAs	Near unity	Above 90	226
113	400×400×80	Two	Au, Si	99.9	Above 90	115
790	400×400×100	Two	W, GaAs	99.84	Above 91	**This work**

5.3.10 Illuminated *J–V* plots of GaAs solar cells

Since the proposed absorber exhibits broadband absorption bandwidth from visible to near-IR regions, it can be used for solar energy harvesting applications. So, in this section we will try to calculate the efficiency for solar applications. Fig. 5.10 demonstrates the photovoltaic *J-V* curve of the proposed metamaterial absorber.. In Fig. 5.8(a), we have already estimated the short-circuit current density (J_{sc}) for both modes at different incident angles. We have calculated the open-circuit voltage (V_{oc}), fill factor (FF), and conversion efficiency (η) for the normal incidence angle. The open-circuit voltage (V_{oc}) is one such parameter that refers to the driving force behind charge separation in a solar cell. V_{oc} can be expected to be large

when the driving force of charge separation is large. V_{oc} formulae are commonly obtained from current-voltage dependency, which can be represented as [186,238,239],

$$V_{oc} = \frac{K_B T}{e} \ln\left(\frac{J_{sc}}{J_o} + 1\right) \tag{5.16}$$

Where K_B, T, e, J_{sc}, and J_o are represents the Boltzmann's constant, temperature, elementary electric charge, short-circuit current density, and reverse saturation current, respectively.

In general, the performance of the solar cell's energy conversion efficiency is said to be the most relevant figure. The calculation of solar cell efficiency can be obtained by dividing the electrical power of the cell at the maximum power (P_{out}) point produced by the input solar radiation (P_{in}) and the surface area of the solar cell. Theoretically, the efficiency of the solar cell can be calculated with the help of Eq. 5.17.

$$\eta = \frac{P_{out}}{P_{in}} = \frac{J_{sc} \times V_{oc} \times FF}{P_{in}} \tag{5.17}$$

Where the incident flux P_{in} is 1000 W/m^2 for the solar spectrum A.M 1.5.

In Fig. 5.2(a), we have already demonstrated the absorption of the GaAs split disk and the complete structure of the metamaterial absorber. The absorption result of only GaAs split disk achieves an average absorption of ~10.93%, while the complete metamaterial absorber structure absorption shows an average absorption of ~96.57%. When the electromagnetic wave hits the GaAs split-disk resonator, most of the light is easily transmitted through the gap and lower surface of the GaAs layer. Therefore, only the GaAs split-disk resonator is not absorbed much energy and shows low absorption. Due to this low absorption, the GaAs split-disk resonator reveals low short circuit current density (J_{sc} =2.46 mA/cm^2) and efficiency (η =1.71%). To control the transmitted electromagnetic waves, we have composed a tungsten

layer on the bottom surface of the GaAs split disk. Due to the greater thickness of the back-layer metal to the skin depth, the layer gives almost zero transmission over the considered optical region. The tungsten layer has a high internal loss which creates strong resonance. It, therefore, contributes more towards ultra-high absorption for the proposed metamaterial absorber structures. Considering the proposed metamaterial absorber, we calculate the short-circuit current density (J_{sc}) and conversion efficiency (η). The observed results are J_{sc} = 44.75 mA/cm^2, and η = 27.33%. If we consider only GaAs split-disk layer as an absorber layer in solar cells, it is not working as a perfect absorber and shows small values of J_{sc} due to minimal absorption. Therefore, the utility of only the GaAs split-disk layer as an absorber layer in solar cell design would not be beneficial. As per the previously reported works[137,186,240], we have considered the total absorption to calculate the short circuit current density as well as efficiency.

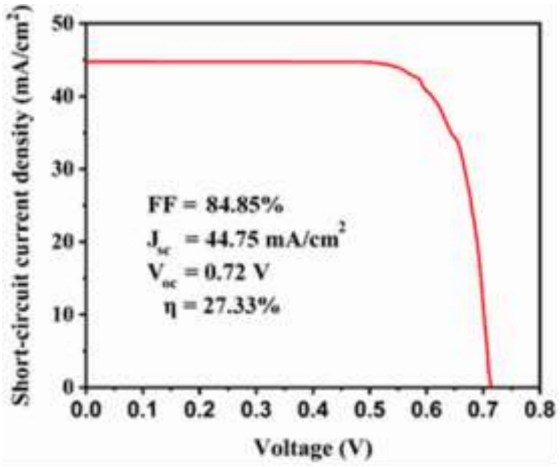

Fig. 5.10 Photovoltaic J-V curves of the proposed metamaterial absorber-based solar cells.

5.4 Conclusion

We have presented a highly efficient broadband absorber and investigated its characteristics with the help of CST software. We have proposed a broadband metamaterial absorber using only two layers consisting of gallium arsenide (GaAs) and tungsten (W) substrates. The structures show an average absorption of 96.57% from the visible to the near-infrared region (375 nm to 1200 nm). We attempted to match the absorber's impedance to the free space's impedance, which is a necessary condition to obtain perfect absorption over the complete region. We have checked the polarization insensitivity performance and found that the change in polarization angle does not significantly affect the absorption rate. In addition, we have also checked the absorption performance at various incident angles ranging from 0^o to 50^o and concluded that our proposed design shows good absorption at all incident angles. The geometry performance has also been investigated to obtain the perfect absorption in the proposed absorber. Furthermore, absorptions from various metals and semiconductors are also investigated to optimize the best absorption for appropriate combinations. We have obtained an average absorption of 95.41% and 96.88% at different incident angles for the TE and TM modes. Moreover, we have calculated the short circuit current density at different angles and obtained an incredible value of around 44.75 mA/cm^2 at a normal incident. We have also evaluated the open-circuit voltage *(V_{oc}),* Fill factor, and conversion efficiency (η) whose values are 0.72 V, 84.85%, and 27.33% respectively. Thus, the proposed metamaterial absorber can be used to design solar harvesting devices and solar cell applications.